Effective Macroion Charge and Stability of Highly Asymmetric Electrolytes at Various Salt Conditions†

Vladimir Lobaskin*

Physics Department, University of Fribourg, CH-1700 Fribourg, Switzerland

Khawla Qamhieh

Physics Department, College of Science and Technology, Al-Quds University, Jerusalem, Palestine

Received: December 3, 2002; In Final Form: April 16, 2003

We study electrostatic mechanisms of the destabilization of highly asymmetric electrolytes. For this purpose, we perform primitive model Monte Carlo simulations of charged macroions immersed in multivalent salt solution. At low salt concentration, the macroion effective charge is reduced due to multivalent counterion adsorption. At high salt concentrations, the macroions become overcharged so that their apparent charge has the opposite sign to the stoichiometric one. The inverted charge increases to a saturation value upon further increase of the salinity. The system remains stable at low as well as at very high salt concentrations. In the intermediate region, close to the macroion isoelectric point, we observe macroion aggregation. The obtained phase behavior closely resembles polyelectrolyte-induced instability of colloidal dispersions.

I. Introduction

Electrostatic interactions in colloidal suspensions and their relation to their phase stability have always attracted much attention because of their occurrence in many biological and technological circumstances. It has been known for a long time that the presence of the oppositely charged macroions seriously deteriorates the stability of colloidal dispersions. In polyelectrolyte-induced aggregation, a correspondence between the location of the fast aggregation regime and the colloid isoelectric point has been documented repeatedly.[1−4] Furthermore, the electrophoretic mobility of colloidal particles, which reflects the apparent particle charge, has been shown to be tightly correlated with the system's stability. The attractive interactions due to surface charge heterogeneities have been thought to promote colloidal aggregation in colloid−polyelectrolyte systems ("charge patch flocculation").[1,2,4] However, it only recently became clear that, apart from specific binding between different solutes and van der Waals forces, the electrostatic correlations themselves can lead to variety of exciting phenomena in systems containing oppositely charged macroions, such as giant charge inversion or short-range attraction between like-charged macroions (meaning either colloids or polyelectrolytes).[5−20] Moreover, computer simulations and theoretical studies have revealed that the correlation-induced attraction can cause macroion aggregation even when only small multivalent ions are present.[8,12,13,16,21] It was shown that the universality of the underlying phenomena is based on the enormous energetic contribution of the Coulombic interactions to the solution's free energy, which dominates over the entropy and makes the system insensitive to the internal structure of the counterions.[10,13,22−25] A phase diagram featuring a phase separation region around the macroion isoelectric point with a consequent restabilization was predicted for a purely Coulombic system containing macroions and a sufficient amount of multivalent counterions.[15,26]

In the present work, we present a computer simulation study of charge inversion and phase instabilities in an asymmetric electrolyte treated by a multivalent salt. This model is meant as a generic representation of a solution containing two types of oppositely charged macroions. We hope to recover the basic properties of such a system originating from the electrostatics and translational degrees of freedom of the solutes. Our simulation setup resembles a common experimental situation when an initially stable suspension is destabilized by adding oppositely charged multivalent ions (or polyelectrolyte) and is aimed to outline the range of activity of the "charge patch attraction"[1,2,4] as well as assess the theoretical predictions[15,26,27] for phase behavior of asymmetric Coulombic systems at different electrostatic coupling parameters. This work also complements the recent computer simulation studies of these phenomena[21,24,25,28] by investigation into salt effects and the role of the effective macroion charge.

The paper is organized as follows. In section II, we give the description of the model and parameter settings for the numerical experiment. Section III gives a detailed account of the results for three series of simulations with different charge asymmetries. Section IV presents discussion of the mechanisms of observed phase behavior and its relation to effective interactions between the colloids. The conclusions are given in the final section.

II. Model and Method

A. Model. The systems under consideration are asymmetric electrolytes described within the framework of the primitive model. The reference electrolyte contains two types of spherical charged particles: (i) macroions of diameter $\sigma_M = 40$ Å and charge $Z_M = -60$ and (ii) small ions of diameter $\sigma_I = 4$ Å and charge $Z_I = +1$, representing the counterions, whereas the solvent enters the model only by its relative dielectric permittivity ϵ_r. The added salt consists of small ions of diameter 4 Å:

† Part of the special issue "International Symposium on Polyelectrolytes".

* Corresponding author. Present address: Max Planck Institute for Polymer Research, D-55128 Mainz, Germany. E-mail: Lobaskin@mpip-mainz.mpg.de.

10.1021/jp027608+ CCC: $25.00 © 2003 American Chemical Society
Published on Web 06/28/2003

monovalent anions $Z_a = -1$ and cations of different valencies. We classified the simulated systems by the added cation charge: series A contains cations with $Z_c = +1$, for series B $Z_c = +3$, and for series C $Z_c = +5$. The last two chosen coupling strengths belong to the instability region on the generic phase diagram for the system including only macroions with their counterions.[12,28] The initial 60:1 system was previously studied in refs 28 and 29, and in deionized system with trivalent counterions a phase separation was found.[12,21] We characterize the amount of added salt by a ratio of the overall added cation charge to the overall macroion charge, $\beta = Z_c\rho_c/(Z_M\rho_M)$, where ρ_i is the number density of the corresponding species.

The interaction between the particles in our model is pairwise additive, and for pair *ij*, where *i* and *j* denote either polyion or counterion, it is given by

$$U_{ij}(r) = \begin{cases} \infty, & r < (\sigma_i + \sigma_j)/2 \\ \dfrac{Z_i Z_j e^2}{4\pi\epsilon_0\epsilon_r}\dfrac{1}{r}, & r \geq (\sigma_i + \sigma_j)/2 \end{cases} \quad (1)$$

where r is the center-to-center separation between the particles.

To characterize the intensity of the electrostatic correlations between counterions on the surface, we use the counterion−counterion coupling parameter $\Gamma = Z_l^2 l_b/a_Z$, where $l_b = (e^2/4\pi\epsilon_0\epsilon_r kT)$ is the Bjerrum length, e is the elementary charge, ϵ_0 is the dielectric permittivity of vacuum, and $a_Z = [Z_l/(\sigma/e)]^{1/2}$ is the average distance between two neighboring counterions at the charged surface characterized by the surface charge density σ. It is known that the correlation-induced attraction appears at $\Gamma > \Gamma^* \approx 2$.[7,21,28] Our systems A, B, and C correspond to $\Gamma = 0.8$, 4.1, and 8.8, respectively.

The systems are considered at a fixed macroion number density $\rho_M = 2.5 \times 10^{-7}$ Å^{-3} corresponding to a macroion volume fraction $\phi_M = 0.0084$. A temperature of $T = 298$ K and a relative dielectric permittivity of $\epsilon_r = 78.4$ were used. For each of the three series, 11 values of β ranging from 0.1 to 10 were studied.

B. Method and Simulation Settings. In this study, we applied the multiparticle Monte Carlo (MC) simulation method, which was developed in our earlier works.[29,30] The canonical NVT ensemble with periodic boundary conditions and the Ewald summation for handling the electrostatic interactions were employed. The simulated bulk systems were composed of 20 macroions, 1200 monovalent counterions, and various amounts of added salt ions. Typically, $(0.5-1) \times 10^5$ attempted MC moves per particles were made in the production runs, while for samples at $\beta \approx 1$ we performed up to 1×10^7 moves.

For the simulation of solutions with much salt we combined cluster MC moves for macroions[29] with *swap moves*, which is a modified implementation of the cluster moves. In the swap move, we first select the macroion and determine the particles within a concentric sphere around it. Then a second sphere of the same radius is taken centered at the destination vector of the macroion translational move $\delta\mathbf{r}_M$ and a central inversion of the content of the whole volume within the two (possibly overlapping) spheres about the center of symmetry at $\delta\mathbf{r}_M/2$ is performed. The acceptance ratio is then calculated in the same way as for the standard cluster move,[29] which, in the simplest case of 100% probability of the particle inclusion, forbids the moves that change the number of particles in the cluster (cf. discussion in ref 29). This type of move significantly improves the acceptance ratio for the systems with homogeneously distributed ions in the bulk as the macroions always move into an ion-free volume.

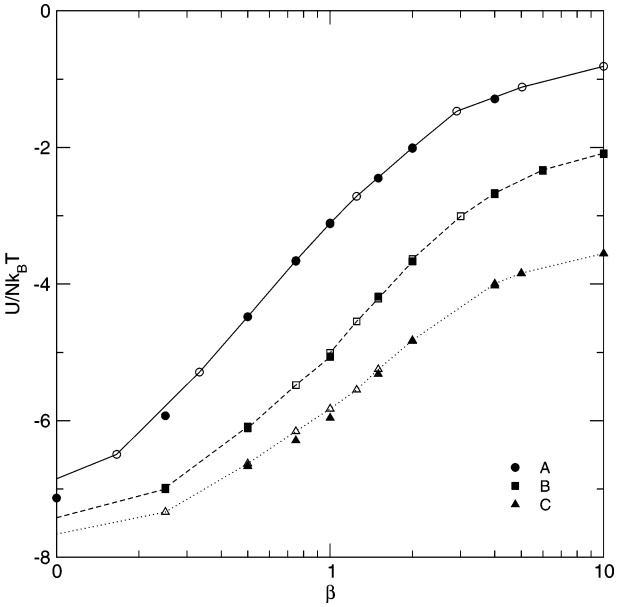

Figure 1. Reduced electrostatic energy for series A, B, and C from bulk MC simulation with 20 macroions (filled symbols) and the corresponding WS cell model (open symbols).

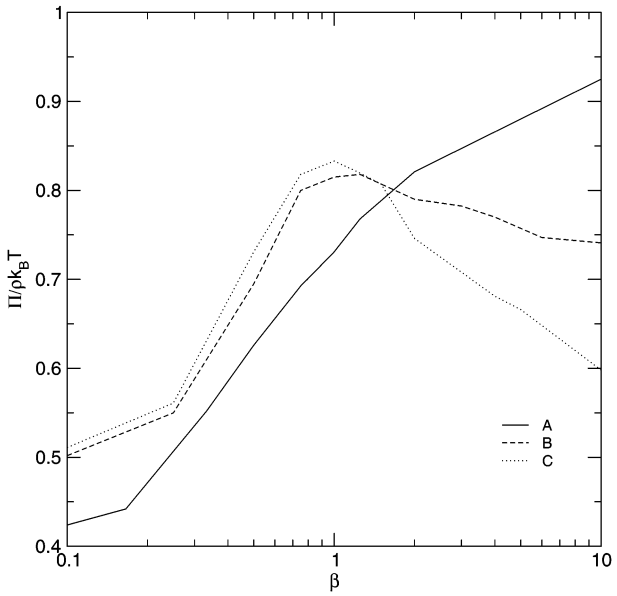

Figure 2. Osmotic coefficient ($\rho(R_{cell}/\rho)$) for series A, B, and C from MC simulation of the WS cell model.

To evaluate the effective macroion charge and the osmotic coefficient, we applied the spherical Wigner−Seitz (WS) cell model. The model was solved by canonical MC simulations for one centrally placed macroion with a corresponding amount of small ions, while the other settings were the same as for the bulk simulation. The simulation package MOLSIM v3.1 by Per Linse et al. was used throughout. Further details of the simulation protocol can be found in refs 29 and 30.

III. Results

A. Single Macroion Properties. Thermodynamics. We begin discussing the numerical results from thermodynamic properties of the chosen electrolytes as a function of the salt concentration. In Figures 1 and 2 we plotted the reduced electrostatic energy of the solution U/Nk_BT and the osmotic coefficient $\Pi/\rho k_BT$, where N and ρ are the total number and the number density of the ionic species, respectively, k_B is the

Boltzmann constant, and Π is the osmotic pressure. The reduced energy was calculated from both bulk simulation and the WS cell model. Figure 1 shows that the total potential energy is negative at all the studied conditions as a result of strong attraction between the macroions and counterions. Its magnitude decreases monotonically with the salt content, which is a simple consequence of increasing the overall number of particles. All the curves have similar shapes with varying curvatures. An inflection point is observed at about $\beta = 1$ on each curve. For the osmotic coefficient shown in Figure 2, we present the cell model results obtained from the total density of ions at the cell boundary $\Pi_{cell}/(\rho k_B T) = \rho(R_{cell})/\rho$. The osmotic coefficient behaves differently for systems A and systems B and C. For system A, it increases roughly proportionally to $\ln \beta$ up to $\beta = 1$, and after that more slowly approaches unity, the ideal solution value. In the two latter series it again grows proportional to $\ln \beta$ at low salt but with slightly higher coefficient. Curves for both series B and C have a peak at $\beta = 1$ and then decrease proportionally to $-\ln \beta$, with the decay of series C results being faster. The value of the osmotic coefficient at the peak is about 0.8. The proximity of the β values to unity in all these cases reflects the high fraction of free ions in the solution. This fraction can be roughly estimated as $(N_a + N_c + Z_{eff} + N_M)/N$, which at $\beta = 1$ for complete adsorption of the added cations gives 121/181, 121/141, and 121/133, or 0.67, 0.86, and 0.91 for systems A, B, and C, respectively. The further decrease of the osmotic coefficient is a result of association of salt anions with the multivalent cations, which reduces the number of "free" species as compared to the ideal solution value.

B. Single Macroion Properties: Effective Charge. The concept of effective polyion charge attracted much attention in the literature due to its importance for the reduction problem. It immediately arises whenever the solvent- or ion-averaged interactions between solutes are concerned. The two major trends (excluding the experimental definitions) for two-component systems (macroion and counterions) are represented by the thermal and structural definitions. The different definitions in a spherically symmetric case consider the distance from the macroion center, within which the charge should be counted. The structural definitions are based on the knowledge of the radius, at which the mixed macroion−ion radial distribution function (rdf) falls below unity, or other criteria. The simplest of the thermal definitions counts the charge inside the macroion−ion binding radius ($|U(r_{therm})| = kT$). The more accurate one considers the chemical potential of the counterion in the macroion field. In the cylindrical case it was developed by Manning and Oosawa[31,32] and adopted for spherical geometry by Belloni.[33] The radius in this approach is measured at the inflection point of the accumulated running charge curve plotted over inverse distance from the macroion center $1/r$ (see also refs 33 and 35 for discussion of alternative definitions). Obviously, the radius is different for ions of different valencies.

In the case of multicomponent electrolyte, however, we have to apply different definitions to different ionic species due to qualitatively dissimilar behavior of the integrated running charge depending on the salt valency. Here, we use MC simulation to solve the WS cell model[29] and then extract the effective charge out of the integrated running charge curves. For series A and series B, C at low salt concentration, we apply the inflection point method.[33] For $\beta > 1$, where the inflection point was not accessible anymore, we evaluated the effective charge at the first extremum of the integrated running charge curves.

Figure 3 demonstrates typical ionic distribution profiles for systems A, B, and C. While all the curves decay monotonically

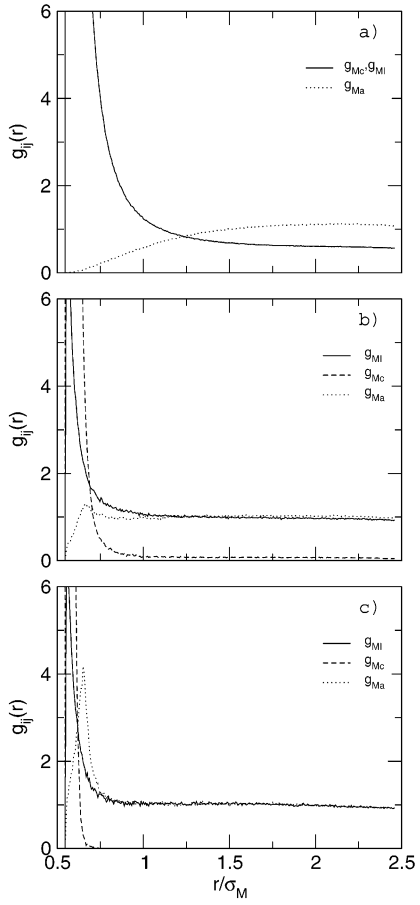

Figure 3. Counterion (g_{MI}) and added salt ion distributions around the macroion (multivalent counterion g_{Mc}, coion g_{Ma}) for the series (a) A, (b) B, and (c) C, as obtained from MC solution of the WS cell model.

in series A, systems B and C display diverse behavior for the different ionic species. The number density of monovalent counterions decays similarly to that of system A. The multivalent ion density has a high maximum at the polyion surface, while farther in the bulk it is close to zero. The coion distribution is peaked close to the maximum of the multivalent ion distribution and becomes very pronounced at high salt concentrations.[36]

The integrated running charge curves are presented in Figure 4. There is a distinct qualitative difference between system A and the two other systems B and C. While in the former one the total charge decays monotonically and reaches zero only at the cell boundary, in the two latter systems the charge exhibits a sharp drop to zero within a very narrow region $r < 1.2\sigma_M$. At $\beta = 1$, the running charge remains close to zero up to the cell boundary. At higher β, the charge changes its sign and after that decays slowly. Close to the cell boundary, one can see the cation charge buildup (note that the charge is divided by negative Z_M), which originates from repulsion between the charge inverted macroions and cations. Note that the accumulated charge in series A at high salt concentrations reaches zero already at $r = 1.5\sigma_M$, which is much less than the mean distance between the macroions.

In Figure 5, we present the effective macroion charge as a function of β for all three series. For all the systems Z_M^{eff}/Z_M starts from about 0.3 at low added salt (its value for the 60:1 electrolyte[29]) and then monotonically decreases. The effective charge changes its sign for systems B and C and regains roughly the same magnitude (0.17 for series B and 0.36 for series C)

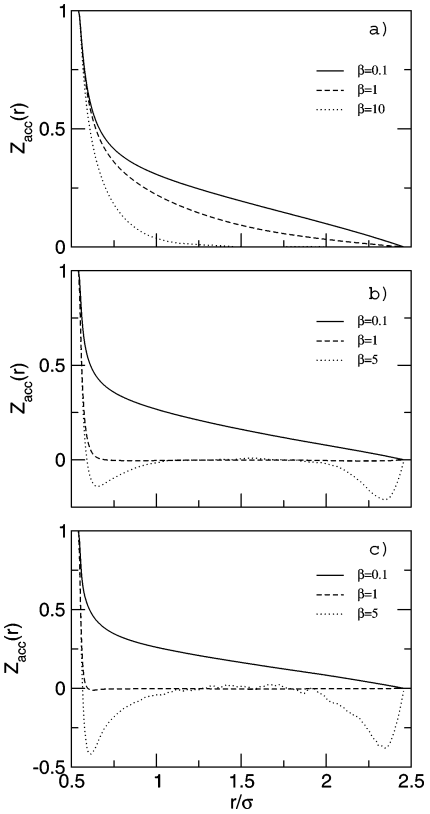

Figure 4. Accumulated running charge as a function of the distance from the macroion center as obtained from MC solution of the WS cell model: (a) series A; (b) series B; (c) series C.

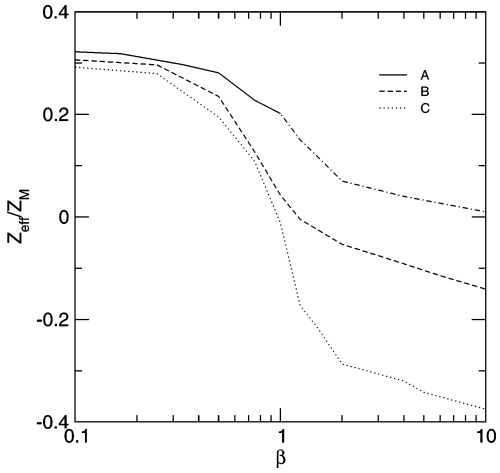

Figure 5. Effective macroion charge for series A, B, and C vs added salt concentration $\beta = Z_c\rho_c/(Z_M\rho_M)$ as obtained from MC solution of the WS cell model. The data for system A at $\beta > 1$ (dotted−dashed curve) are obtained in the region where the definition of the effective charge based on the inflection point criterion is no longer justified.

on the negative side. It is interesting to note the qualitative similarity of all three curves. All of them have two relatively flat regions at very low and very high salt concentrations and a region of fast variation with an inflection point at about $\beta = 1$. The curve for series A asymptotically approaches but never crosses the zero line. Very slow dependence of the effective charge on the salt content at $\beta > 1$ follows from logarithmical increase of the counterion entropy with counterion number density.[26] One should note that the decrease of the effective charge with the salt concentration, as seen for $\beta < 1$, is characteristic for dilute and deionized systems, where the effective charge is far from its saturated value.[33] At the higher monovalent salt content, $\beta > 1$, the ionic double layer saturates and Z_M^{eff}/Z_M starts growing with salt concentration toward unity.[33,34] We could not see this upturn due to the failure of the inflection point criterion in this region. The failure is due to the fact that the underlying division of the ionic population into the "condensed" and "free" parts is no longer valid. The inflection point can still be detected formally, but it refers now to the far field properties of the double layer (the inflection point is located next to the cell boundary) and does not reflect its short-range decay, which is important for interaction between the macroions.

C. Collective Macroion Properties: Structure. The object of our main interest here is the macroionic distribution. We therefore analyze only macroion−macroion partial distributions and extract those data that characterize the macroion density fluctuations. Namely, we consider the long wave limit value of the macroion−macroion partial structure factor $S_{MM}(q)$, which would quantify the reduced osmotic compressibility in a corresponding one-component fluid of macroions. We should note that due to the small size of the simulated sample we can access only a relatively short-wave region ($q\sigma_M > 0.01$) and therefore have only a rough estimate of $S_{MM}(0)$. One should expect stronger deviations from unity for the true $S_{MM}(0)$, i.e., even lower values for the stable solutions and the higher ones for the aggregating systems.

The macroion distribution in the bulk solution can be easiest illustrated by simulation snapshots shown in Figure 6. Snapshot a corresponds to a low added salt content $\beta = 0.1$ and reveals a homogeneous spatial distribution of the macroions. In snapshot b corresponding to $\beta = 1$ one can see macroion clusters. All the macroions are in aggregated state. Finally, snapshot c demonstrates that at high salt $\beta = 5$ most macroions are free and the solution is back to the stable state. The cluster redissolution is in agreement with theoretical predictions[26] and recent simulations for polyelectrolyte-induced aggregation of colloids and globular proteins.[24,25] We should note that even at high β values occasional particle pairs are formed. To ensure the equilibrium thermodynamic state of the system, we performed additional simulations with initial compact configuration of the macroions. The macroions were allowed to move after the equilibration of the ionic subsystem. Then, indeed we observed stable aggregates at $\beta \approx 1$ and redissolution of the macroions at the higher salt dose. The parameters of the aggregates were drifting slowly toward their values from the simulation with random initial configuration with an increase of simulation length. The difficulty with matching the two sets of data for the redissolution and the cluster−cluster aggregation is caused by the wide energy barriers originating from the large net charge of the clusters.[37] Although the cluster charge does not grow proportionally to the number of macroions due to the partial counterion release, it yet reached values of $2Z_M^{eff}$ in our systems B and C at $\beta > 1$.

Figure 7 presents partial macroion−macroion radial distribution functions (rdf) for the three systems at different salt concentrations. In Figure 7a, one can see the results for system A, which show gradual decay of the macroion ordering on increasing salt. The peak of the rdf appears initially at $r = \rho^{-1/3}$ and has a value of 1.15, and then moves toward shorter separations, while decreasing at the same time, and almost disappears at $\beta > 1$. The trend is readily understood from decreasing the effective macroion charge and increasing the screening ability of the electrolyte at the higher salt contents. For the remaining two series B and C, the trend is very different. Already at $\beta = 0.5$ there is a peak near the macroion contact

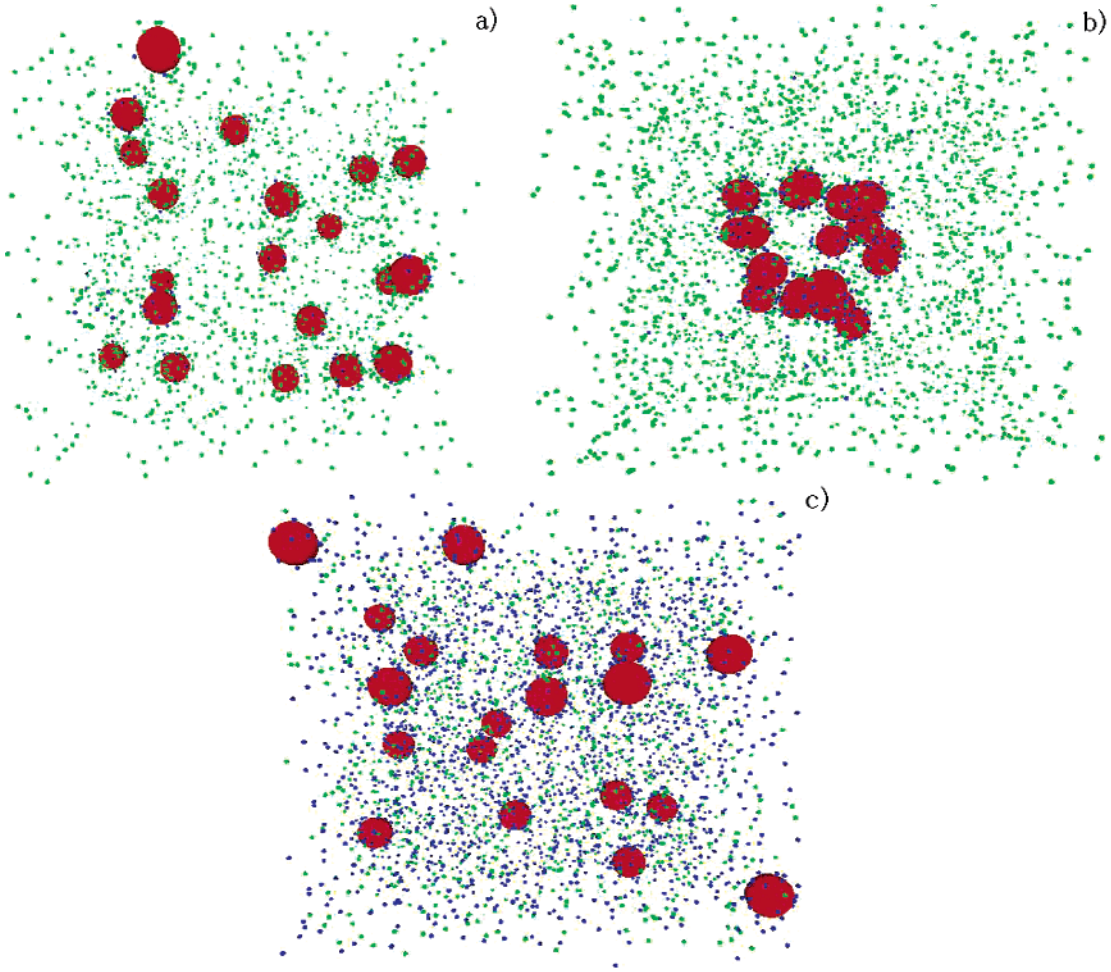

Figure 6. Snapshots of the primary simulation box for series C with 20 macroions taken at the end of simulation at (a) $\beta = 0.1$, (b) $\beta = 1$, and (c) $\beta = 5$. The big spheres represent the macroions; the small ones represent the counterions and added salt ions. The coions are omitted in (c) for clarity. In (b) corresponding to $\beta = 1$, one can see macroion cluster.

distance (or, more exactly, at $r = \sigma_M + \sigma_c$), which then grows high upon salt addition and reaches the value of 60 at $\beta = 1$ for series B and 150 for series C. At $\beta > 1$ it considerably drops in height but still remains quite high even at $\beta = 10$. A secondary peak at $r = 2\sigma_M$ corresponding to the second particle layer in a cluster is seen for some of the curves in series B and C at $\beta > 1$. We note the reappearance of the remote peak at $r = 5\sigma_M$ for series C at $\beta = 10$. We made also another interesting observation for system C. At salt concentrations $\beta \geq 1$, the main peak of the macroion−macroion rdf shifts toward $r = \sigma_M$ and is seen now at $r = 1.02\sigma_M$ instead of $r = \sigma_M + \sigma_c = 1.1\sigma_M$. This effect might be related to strengthening the electrostatic depletion contribution to the macroion interaction.[9]

We plotted some macroion−macroion partial structure factors for different salt concentrations in Figure 8. The structure factors for series A again shows decay of the structure on increasing β. For the two remaining series, the structure factors have initially a peak at $q\sigma_M = 2$ that corresponds to the inverse mean distance between the macroions and a low value in the long-wave limit. On increasing salt concentration, this peak disappears and two new peaks develop instead at $q\sigma_M \rightarrow 0$ and $q\sigma_M \approx 7$. The first peak reflects the average macroionic cluster size that grows with the salt addition until $\beta \approx 1$ for series B and C. After that, when even more salt is added, the value of the long-wave peak decreases, which indicates the redissolution of the clusters. The broad secondary peak at $q\sigma_M \approx 7$ corresponds to the macroion−macroion density buildup close to contact distance.

The whole set of values of the long-wave structure factor value $S(0)$ for all three series is shown in Figure 9. The curve for system A shows a gradual increase between $\beta = 0$ and 10 while the curves for systems B and C have well expressed maxima around $\beta = 1$. For system B, the peak is slightly shifted toward higher salt concentration due to the competition between the adsorption energy and the cation entropy, which leads to incomplete macroion charge compensation at $\beta = 1$. For series C, the $S(0)$ value returns to values less than 1, as it was at $\beta \ll 1$. The overall trend for system C corresponds to its destabilization at $\beta \approx 1$; a consequent restabilization at high salt concentration occurs due to recovery of the repulsion between the macroions (cf. the effective charge plot in Figure 5).[15,26]

IV. Discussion

As we have seen from the above results, the salt conditions are crucial for the stability of asymmetric electrolytes. On the path along the salt concentration axis, two important parameters of macroion interactions are affected: the Debye screening length and the effective charge of the macroions. The effect of the former is rather smooth and can be detected through a simple damping of the interactions upon salt addition. The sensitivity of the asymmetric electrolyte to the added salt depends also on the relative amounts of the "native" and "added" ions. We note that overall properties of the studied systems mark the charge compensation point $\beta = 1$ either by an extremum (the osmotic coefficient) or an inflection (potential energy, effective charge),

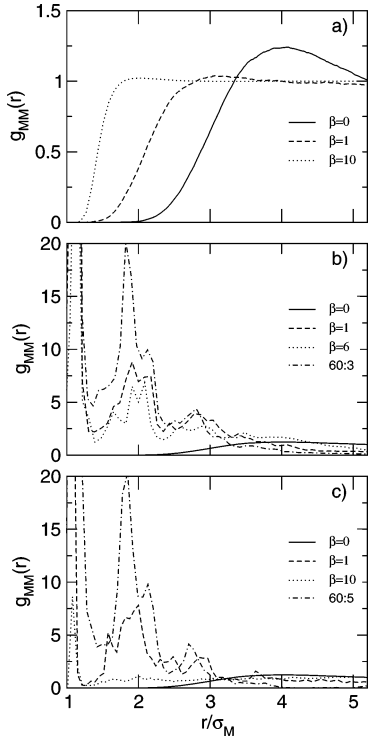

Figure 7. Macroion−macroion partial radial distribution functions for series (a) A, (b) B, and (c) C at the indicated added salt concentrations given in units of $\beta = Z_c\rho_c/(Z_M\rho_M)$ from MC simulation with 20 macroions. The curves obtained for asymmetric electrolytes 60:3 and 60:5 without monovalent ions are given for comparison (see discussion in section IV). The stripped initial maxima have values of 60 and 150 for series B and C, and 200 and 230 for 60:3 and 60:5 systems, respectively.

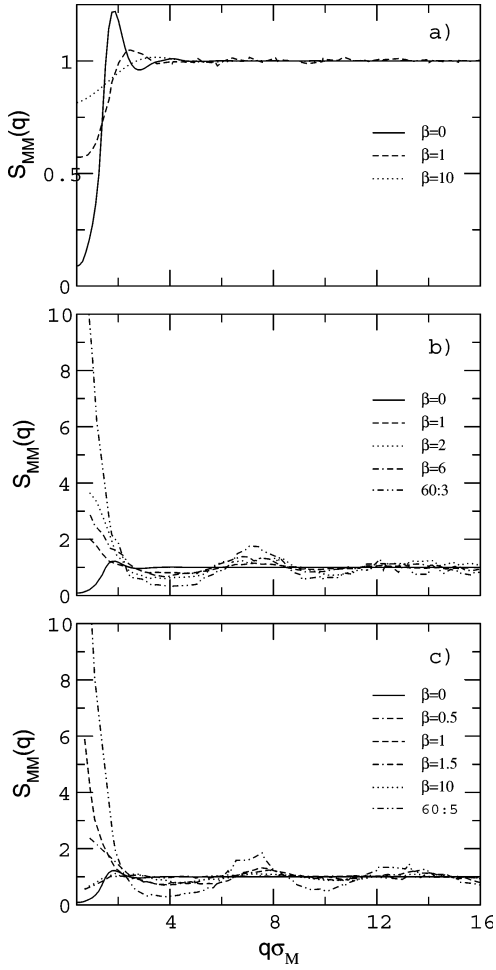

Figure 8. Macroion−macroion partial structure factors for series (a) A, (b) B, and (c) C at the indicated added salt concentrations given in units of $\beta = Z_c\rho_c/(Z_M\rho_M)$ from MC simulation with 20 macroions. The curves obtained for asymmetric electrolytes 60:3 and 60:5 without monovalent ions are given for comparison (see discussion in section IV).

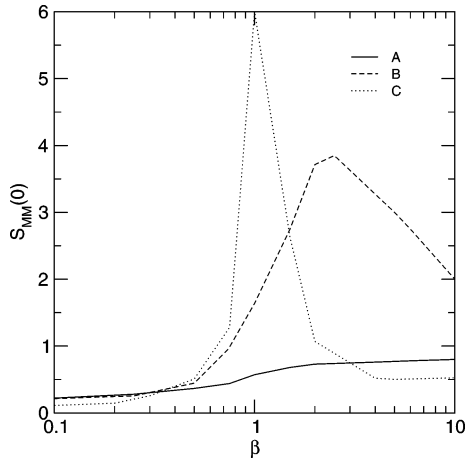

Figure 9. Long-wave value of the macroion−macroion partial structure factor ($S_{MM}(0)$) for series A, B, and C from MC simulation with 20 macroions.

which can be understood as a crossover from the counterion-dominated ($\beta < 1$) to the salt-dominated screening ($\beta > 1$).

Another interaction parameter, the effective charge, influences mostly the macroion-related properties such as the macroion distribution and the stability of the macroion subsystem. In the counterion-dominated regime, the effective charge changes almost linearly with the salt concentration. This makes the system extremely sensitive to the addition of salt. In contrast, at the higher electrolyte strength the effective charge increases logarithmically with the amount of added multivalent salt. We note a close similarity between the observed charge behavior and the macroion electrophoretic mobility vs added polyelectrolyte dose curves reported in refs 3 and 4. Figure 10 demonstrates the direct relation between the effective charge and the stability of the electrolyte solution. In the plot one can see the relative effective charge curve together with the characteristics of stability $S_{MM}(0)^{-1}$ for series C. It is important to note the approximate symmetry of the curves in Figure 10 relative to the isoelectric point, which allows one to formulate the result in a symmetric manner. While one can say that on the right-hand side of the diagram the macroions are overcharged by the excess multivalent counterions, on its left-hand side there is excess of macroions themselves and they are overcharging the multivalent ions. The latter has a richer physical meaning when we imagine polyelectrolyte molecules instead of multivalent ions. The effect of the internal counterion structure was discussed recently.[22,24] As shown previously for the asymmetric electrolytes without added salt,[28] the parameters of importance are the charge asymmetry between the oppositely charged ionic species and the ion correlation parameter Γ. Extending our conclusions, we should expect that strongly charged systems with similar energetic parameters have common features irrespective of the internal structure of the polyions, whether they are polyelectrolytes or colloids.

While changing the salt valency leads to a smooth variation of the system's properties such as the internal energy, osmotic coefficient, or effective macroion charge at the salt-overdosed

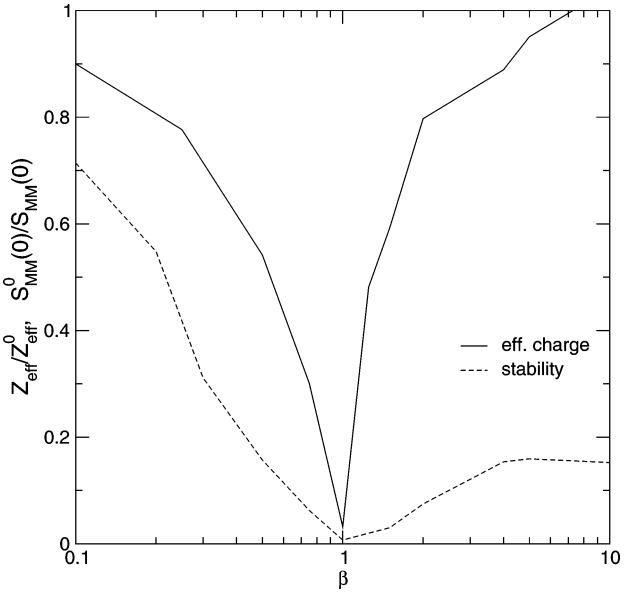

Figure 10. Absolute value of effective macroion charge and the stability ratio ($S_{MM}(0)^{-1}$) for series C normalized by their values at $\beta = 0$.

conditions far from the isoelectric point, the interactions and structure change drastically in all the series at $\beta = 1$. Our results confirm that the instability appears at a certain threshold counterion valency and becomes sharper at the higher counterion charge (or counterion coupling Γ). Therefore, at the higher Γ one can expect, on one hand, a much stronger macroion aggregation at $\beta = 1$ and, on the other hand, a much better expressed overcharging and redissolution effects. Thus, the three systems of our choice correspond to (i) the weak coupling region and counterion entropy dominated behavior (series A), (ii) the border region demonstrating the coexistence of condensed and free counterions at $\beta = 1$ (series B), and (iii) the high coupling (or "low temperature") regime with completely condensed multivalent counterions (series C). The latter case was analyzed in detail recently.[26] At the same time, the instability in real solutions should be much enhanced due to van der Waals forces, which due to their short-range character similarly play a role only in the vicinity of the isoelectric point; i.e., the whole sequence must be shifted toward lower Γ values.[25]

Finally, we report on the simple salt effect on the effective charge and the counterion correlation attraction. The salt effects in similar systems were discussed previously.[21] It was confirmed that the added salt screens the repulsions between the macroions and leads to weakening the long-range macroion ordering. In a 60:2 electrolyte, addition of divalent ions caused an increase of the electrostatic attraction. In the 60:3 electrolyte, which is similar to our system B but has no monovalent counterions, no significant effect was noticed. Basing on the above analysis, we can explain the increase of the macroion aggregation in the 60:2 electrolyte as that the added divalent ions in fact lessen the effective macroion charge, which is not compensated completely at $\beta = 1$ (similar to system B of the present work at $\beta = 1$).[38] The apparent salt effect in the 60:3 electrolyte was small because the considered salt concentrations placed the system in the center of the instability region, where it is not very sensitive to the salt. The salt concentration range in ref 21 corresponds to $1 < \beta < 4$ in the current work (cf. the curve for system B in Figure 9). Now, we repeat the comparisons of ref 21 between solutions B and C at $\beta = 1$ and corresponding systems with multivalent ions only, namely 60:3 and 60:5 electrolytes.

In the 60:3 system, the absolute potential energy per macroion is about 2.5% smaller than in series B, while the difference is about 3.3% between the 60:5 electrolyte and system C. Similar relations hold for the partial electrostatic energies: the macroion−cation and cation−cation energies, respectively, are 3.3% and 5.5% higher in the 60:3 solution than in series B at $\beta = 1$. For the 60:5 solution and system C, these differences are marginal: the macroion−cation energy is 0.3% greater in the former, while the cation−cation energy is the same within statistical uncertainty. The osmotic coefficient calculated in the cell model in the 60:5 system is equal to zero, which means that all the multivalent ions are adsorbed and the bulk osmotic coefficient is then just $\Pi/(\rho_M k_B T) \approx 0.08$. The simulation for the 60:3 electrolyte showed about 5 times higher cation concentration in the bulk for the corresponding system B, though both concentrations were very small. At the same time, the presence of the monovalent ions leads to a very modest decrease in correlation between the multivalent ions. The cation−cation correlation peak in system B falls by about 10% with respect to 60:3 electrolyte, which corresponds to a slight decrease of the effective correlation parameter Γ. In system C compared to the 60:5 system, the analogous decrease is just about 5%. The macroion−cation rdf's display marginal sensitivity to the presence of monovalent ions. The peak height is only 5% higher in the 60:3 system, and 2% higher in the 60:5 system than for the corresponding samples B and C.

The relative effective charge Z_M^{eff}/Z_M for both charge asymmetries increases in magnitude with salt addition. With trivalent ions, it rises from $0.015Z_M$ in the 60:3 system to $0.03Z_M$ in system B. For pentavalent ions, it changes from 0 in 60:5 electrolyte to $-0.01Z_M$ in system C. Note that the presence of the anion layer around the adsorbed cations does not cancel the effect (see Figure 3). A significant role here is played by the monovalent counterions, which also accumulate close to the macroion surface. The macroion structure displays considerable sensitivity to the presence of monovalent ions. In the 60:3 system, the first peak of the macroion−macroion rdf increases from 60 to 200 as compared to system B (Figure 7b). The structure factor value $S_{MM}(0)$ rises from 2.1 to 13 (Figure 8b). For the case of pentavalent ions, the rdf peak rises from 150 to 230 (Figure 7c), while the initial structure factor peak rises from 6 to 13 (Figure 8c). One can see from Figure 7b,c and Figure 8b,c that the aggregation is much more strongly expressed in both 60:3 and 60:5 electrolytes than in the corresponding systems B and C. This drastic change can be attributed to (i) the decrease of the effective correlation parameter Γ for the multivalent ions in the presence of monovalent ones and (ii) the change in the macroion effective charge, which has slightly higher magnitude for the systems with monovalent ions present. The accumulation of these small but finite macroion charges opposes the cluster−cluster aggregation and prevents formation of very large clusters.

V. Conclusion

We performed a numerical study of highly asymmetric electrolyte solutions containing strongly charged macroions and different amounts of salt. The addition of a simple monovalent salt gradually lowers the effective macroion charge and reduces the solution stability. Addition of small amounts of multivalent salt produces a similar effect. The dose of multivalent salt that exceeds the macroion isoelectric concentration causes macroion charge inversion and electrostatically driven macroion aggregation. At the isoelectric point, we observe formation of large macroion clusters. When the inverted macroion charge becomes

large enough, the clusters redissolve. Enlarging the counterion valency strenghens the instability at the isoelectric point but stabilizes the solution at the overdosed conditions. The obtained stability diagram closely resembles polyelectrolyte-induced colloidal aggregation, while the aggregation mechanism is related solely to electrostatic correlation forces rather than the van der Waals attractions.

Acknowledgment. We are grateful to Per Linse, Boris Shklovskii, Toan Nguyen, Michal Borkovec, Christian Holm, Yan Levin, Mario Tamashiro, and Peter Schurtenberger for stimulating discussions. This work was financially supported by the Swiss National Science Foundation.

References and Notes

(1) Gregory, J. J. *J. Colloid Interface Sci.* **1973**, *42*, 448.
(2) Miclavic, S. J.; Chan, D. Y. C.; White, L. R.; Healy, T. W. *Langmuir* **1994**, *98*, 902.
(3) Walter, H. W.; Grant, S. B. *Colloids Surf., A* **1996**, *119*, 229.
(4) Bouyer, F.; Robben, A.; Yu, W. L.; Borkovec, M. *Langmuir* **2001**, *17*, 5225.
(5) Guldbrand, L.; Jönsson, B.; Wennerström, H.; Linse, P. *J. Chem. Phys.* **1984**, *80*, 2221.
(6) Gronbech-Jensen, N.; Beardmore, K. M.; Pincus, P. *Physica A* **1998**, *261*, 74.
(7) Rouzina, I.; Bloomfield, V. A. *J. Phys. Chem.* **1996**, *100*, 9977.
(8) Hribar, B.; Vlachy, V. *Biophys. J.* **2000**, *78*, 694.
(9) Allahyarov, E.; D'Amico, I.; Löwen, H. *Phys. Rev. Lett.* **1998**, *81*, 1334.
(10) Kjellander, R. *Chem. Phys. Lett.* **1984**, *112*, 49.
(11) Wu, J.; Bratko, D.; Blanch, H. W.; Prausnitz, J. M. *J. Chem. Phys.* **1999**, *111*, 7084.
(12) Linse, P.; Lobaskin, V. *Phys. Rev. Lett.* **1999**, *83*, 4208.
(13) Shklovskii, B. *Phys. Rev. Lett.* **1999**, *82*, 3268.
(14) Netz, R. R.; Orland, H. *Europhys. Lett.* **1999**, *45*, 726.
(15) Nguyen, T. T.; Rouzina, I.; Shklovskii, B. I. *J. Chem. Phys.* **2000**, *112*, 2562.
(16) Messina, R.; Holm, C.; Kremer, K. *Phys. Rev. Lett.* **2000**, *85*, 87; *Phys. Rev. E* **2001**, *64*, 021405.
(17) Grosberg, A. Yu.; Nguyen, T. T.; Shklovskii, B. I. *Rev. Mod. Phys.* **2002**, *74*, 329.
(18) Levin, Y. *Physica A* **1999**, *265*, 432; *Rep. Prog. Phys.* **2002**, *65*, 1577.
(19) Vlachy, V. *Annu. Rev. Phys. Chem.* **1999**, *50*, 145.
(20) Hansen, J.-P.; Löwen, H. *Annu. Rev. Phys. Chem.* **2000**, *51*, 209.
(21) Linse, P.; Lobaskin, V. *J. Chem. Phys.* **2000**, *112*, 3917.
(22) Reščič, J.; Linse, P. *J. Phys. Chem. B* **2000**, *104*, 7852.
(23) Skepö, M.; Linse, P. *Macromolecules* **2003**, *36*, 508.
(24) Jonsson, M.; Linse, P. *J. Chem. Phys.* **2001**, *115*, 10975.
(25) Carlsson, F.; Malmsten, M.; Linse, P. *J. Am. Chem. Soc.* **2003**, *125*, 3140.
(26) Nguyen, T. T.; Shklovskii, B. I. *J. Chem. Phys.* **2001**, *115*, 7298.
(27) Harnau, L.; Hansen, J.-P. *J. Chem. Phys.* **2002**, *116*, 9051.
(28) Linse, P. *Philos. Trans. R. Soc. London, Ser. A* **2001**, *359*, 853; *J. Chem. Phys.* **2000**, *113*, 4359.
(29) Lobaskin, V.; Linse, P. *J. Chem. Phys.* **1999**, *111*, 4300.
(30) Lobaskin, V.; Linse, P. In *Simulation and visualization on the grid*; Lecture Notes in Computational Science and Engineering 13; Springer: Berlin, 2000; p 165.
(31) Manning, G. *J. Chem. Phys.* **1969**, *51*, 924.
(32) Oosawa, F. *Biopolymers* **1968**, *6*, 1633.
(33) Belloni, L. *Colloids Surf., A* **1998**, *140*, 227.
(34) Bocquet, L.; Trizac, E.; Aubouy, M. *J. Chem. Phys.* **2002**, *117*, 8138.
(35) Deserno, M.; Holm, C.; May, S. *Macromolecules* **2000**, *33*, 199.
(36) Tanaka, M.; Grosberg, A. Yu. *J. Chem. Phys.* **2001**, *115*, 567.
(37) Nguyen, T. T.; Shklovskii, B. I. *Phys. Rev. E* **2002**, *65*, 031409.
(38) Lobaskin, V.; Lyubartsev, A.; Linse, P. *Phys. Rev. E* **2001**, *63*, 020401.